

Towards an Autonomous Efficient Materials Discovery Framework: An Example of Optimal Experiment Design Under Model Uncertainty

Anjana Talapatra^{1,*}, S. Boluki², T. Duong¹, X. Qian², E. Dougherty², and R. Arróyave^{1,3}

¹ *Department of Materials Science & Engineering, TAMU, USA, 77843*

² *Department of Electrical and Computer Engineering, TAMU, USA, 77843 and*

³ *Department of Mechanical Engineering, TAMU, USA, 77843*

(Dated: June 3, 2022)

The accelerated exploration of the materials space in order to identify configurations with optimal properties is an ongoing challenge. Current paradigms are typically centered around the idea of performing this exploration through high-throughput experimentation/computation. Such approaches, however, do not account for—the always present—constraints in resources available. Recently, this problem has been addressed by framing materials discovery as an optimal experiment design. This work augments earlier efforts by putting forward a framework that efficiently explores the materials design space not only accounting for resource constraints but also incorporating the notion of model uncertainty. The resulting approach combines Bayesian Model Averaging within Bayesian Optimization in order to realize a system capable of autonomously and adaptively learning not only the most promising regions in the materials space but also the models that most efficiently guide such exploration. The framework is demonstrated by efficiently exploring the MAX ternary carbide/nitride space through Density Functional Theory (DFT) calculations.

Keywords: Materials Discovery; Bayesian Optimization; Bayesian Model Averaging

I. INTRODUCTION

A. Motivation

The accelerated exploration of the Materials Design Space (MDS) has been recognized for more than a decade as a key enabler for potentially transformative technological developments [1, 2]. The development of strategies to integrate simulations and experimental data with expert knowledge is a highly active area of research [3, 4]. Over time, different methods have been deployed within conventional, human-centric, materials development frameworks for exploration of the MDS, including high-throughput (HT) experimentation and computation.

Current HT experimental [5–7] and computational [8] approaches, while powerful, have important limitations as they: (1) are incapable of dealing with the high dimensionality (compositional, configurational, and microstructural degrees of freedom) and complexity (e.g., multi-physics) of the MDS; (2) employ hardcoded workflows and lack flexibility to iteratively learn and adapt based on the knowledge acquired to assure balanced exploration and exploitation of the MDS; (3) preclude expansion of the MDS—i.e., identification of new materials features— as new information is acquired; (4) are suboptimal in

resource allocation as experimental decisions do not account for the cost and time of experimentation.

Resource limitation cannot be overlooked as it is often the case that once a bottleneck in HT workflows has been eliminated (e.g. synthesis of ever more expansive materials libraries), another one suddenly becomes apparent (e.g. need for high-resolution characterization of materials libraries). Regardless of how many bottlenecks are eliminated, the fact that ultimately a human must make decisions about what to do with the acquired information implies that HT frameworks face hard limits that will be extremely difficult to overcome. On the computational front, there exist significant fundamental and technological challenges to the (multi-scale) simulation of materials [9] that effectively preclude the HT exploration of MDS beyond the use of (sophisticated) methods—such as DFT-based HT simulations [8]—operating at one scale, with relatively small numbers of degrees of freedom.

B. Efficient Materials Discovery

Resource constraints thus call for the *efficient* evaluation of materials configurations in order to identify regions in the MDS with the *optimal response*. Mathematically, this can be framed as finding [11] a global minimizer of an *unknown* objective

* anjanatalapatra@tamu.edu

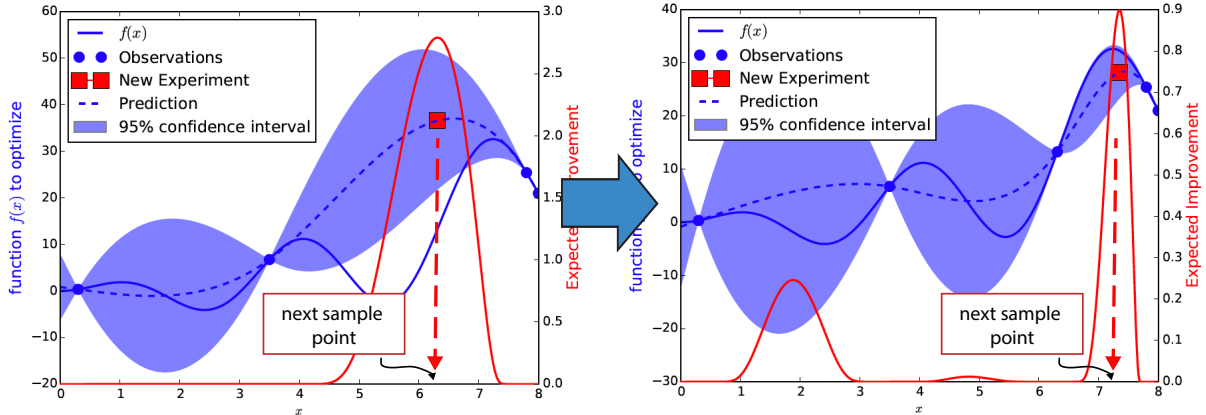


FIG. 1: Schematic illustration of Bayesian Optimization (BO): from a limited number of observations on a system (blue solid line) a stochastic model (dashed blue line and shaded area) is built. The next observation is determined by accounting for the tradeoff between the exploitation of the current knowledge and the exploration of the unknown regions of the design domain x . In this case, Expected Improvement (EI) is the metric used and thus the policy falls within the Efficient Global Optimization (EGO) framework [10].

function f :

$$\mathbf{x}^* = \arg \min_{\mathbf{x} \in \chi} f(\mathbf{x}) \quad (1)$$

where χ denotes the MDS. In the context of materials discovery, f is necessarily a *blackbox function* without a known closed form. Moreover, the cost of querying such a function (through expensive experiments/simulations) at arbitrary query point \mathbf{x} in χ is high and f can only be observed through noisy observations y . Bayesian Optimization (BO) [11, 12] provides a sequential model-based approach to solve the problem: first, a prior belief is prescribed over the objective function and then the model is sequentially refined via Bayesian posterior updating. The domain χ is sampled for a query point \mathbf{x}_{n+1} such that an acquisition function $u(\mathbf{x}; \mathcal{D}_n)$ —constructed from a model of the observed data \mathcal{D}_n —is maximized—see Algorithm 1 and Fig. 1.

Having mapped the exploration of the MDS to an expensive *blackbox function*, several groups have already demonstrated the power of Bayesian Optimization in the context of *accelerated materials discovery*. Early on, Fujimura *et al.* [13] combined DFT and experimental data to construct a model to predict the ionic conductivity of Li-super ionic conductors via Support Vector Regression (SVR) [14]. The predicted conductivity σ_{Li} from the SVR model was then used as the *acquisition function* to further explore the Li-super ionic conductor space. Seko *et al.* [15] used feature sets derived from DFT calculations and experimentally measured melting

points T_m to fit stochastic models based on SVR or Gaussian Process Regression (GPR) [16] to discover unary and binary crystals with the highest melting point. In that case, the acquisition function used in the sequential exploration of the melting point space χ_{T_m} was the *probability* of improving upon the best value recorded before acquisition $n + 1$. These early results introduced the notion of sequential exploration but did not consider the larger implications of framing the materials discovery as the optimization of an expensive *blackbox function*.

Algorithm 1 Bayesian Optimization

- 1: Initialize \mathcal{D}_0
- 2: **for** $n=0, 1, \dots$ **do**
- 3: Select new \mathbf{x}_{n+1} by optimizing acquisition function u :

$$\mathbf{x}_{n+1} = \arg \max_{\mathbf{x} \in \chi} u(\mathbf{x}; \mathcal{D}_n)$$

- 4: Query blackbox function f to obtain y_{n+1}
 - 5: Augment data $\mathcal{D}_{n+1} = \{\mathcal{D}_n, (\mathbf{x}_{n+1}, y_{n+1})\}$
 - 6: Update statistical model
 - 7: **end for**
-

Balachandran *et al.* [17] prescribed the need to balance the need to exploit our current knowledge of the MDS χ with the need to explore it. The balance between exploitation and exploration was realized by invoking a proper acquisition function. Balachandran *et al.* proposed using *Expected Improvement* [10], *EI*, in the predicted objective function y by the model $P(y|\mathbf{x}, \mathcal{D})$ over the unexplored re-

gions of χ , given the observed data \mathcal{D} . EI can in turn be calculated for unexplored query points \mathbf{x} by the model trained. They demonstrated their design protocol by attempting to predict the MAX phases (ternary layered carbides/nitrides [18]) with maximal/minimal polycrystalline bulk/shear moduli as predicted via DFT calculations. Having demonstrated the power of Bayesian Optimization in materials discovery, the same group [19] notably employed the same approach to discover, *via experiments*, NiTi-based Shape Memory Alloys (SMAs) with record-low hysteresis through a minimal experimental effort.

The principled nature of a BO-based materials discovery protocol is amenable to develop full-loop platforms, particularly when attempting to carry out simulation-driven materials development. Indeed, Ju *et al.* [20] recently proposed a framework whereby atomistic transport calculations were combined with a BO framework to identify aperiodic nano-structures with optimal transport properties by examining only an extremely small fraction of the possible configurations. On the experimental front, Nikolaev *et al.* [21] recently demonstrated a fully autonomous closed-loop iterative materials experimentation platform. They demonstrated the system by optimizing the synthesis conditions for carbon nanotubes. In their case, the approach focused on a *greedy* exploitation of the synthesis space by using the acquisition function — the predicted rate of growth—i.e. no exploitation-exploration trade-off [17, 19] was used.

While existing computational and experimental deployments of optimal materials discovery constitute significant advances, there are still significant challenges that remain to be addressed. For example, most BO-based approaches rely on a feature selection step [17, 22] that necessarily requires a considerable number of feature-property sets to be effective [23]. In other cases, the strength of the approach depends on building sufficient prior knowledge (from informative predictive models [15]) in order for *greedy* approaches to be practical.

Unfortunately, more often than not, the amount of relevant data available before embarking on a materials discovery problem is small. In such situations the nature (and dimensionality) of the design space— χ in the BO formalism—is not known *a priori*. Moreover, it is not even clear which features are best connected to the target performance metric. Finally, the inability of existing approaches to ‘*both build and exploit their internal models, with minimal human hand-engineering*’ [24] precludes the implementation of truly autonomous materials discovery

systems, even in simulation-driven approaches.

In this work, we propose a framework that, simultaneously (i) accounts for the need to adaptively build increasingly effective models for the accelerated discovery of materials while (ii) accounting for the uncertainty in the models themselves. We frame the problem as that of Bayesian Optimization under Model Uncertainty (BOMU). The resulting approach incorporates Bayesian Model Averaging (BMA) within Bayesian Optimization in order to realize a system capable of autonomously and adaptively learning not only the most promising regions in the materials space but also the models that most efficiently guide such exploration. The framework is also capable of defining optimal experimental sequences in cases where multiple objectives must be met—to the best knowledge of these authors no prior work on optimal materials discovery considers the multi-objective problem. The framework is then demonstrated by efficiently exploring the MAX ternary carbide space through DFT calculations.

II. BAYESIAN OPTIMIZATION UNDER MODEL UNCERTAINTY

Small sample sizes are ubiquitous in materials science. Experiments—and simulations—are often resource-intensive and this imposes significant constraints on any attempt to explore/exploit the MDS. Moreover, in the absence of sufficient information, there are, *a priori*, multiple features that are potentially predictive of the material performance metric of interest. In all the well-known experiment design methods in the literature, one must select the model (the set of predictive features) before starting the experiment design loop.

Unfortunately, due to small sample size and large number of potential predictive models, the model selection step may not result in the true best predictive model for efficient Bayesian Optimization [25, 26]. It has been shown that small sample sizes pose a great challenge in model selection due to inherent risk of imprecision and overfitting [25, 26], and no feature selection method performs well in all scenarios when sample sizes are small [27]. Thus, by selecting a single model as the predictive model based on small observed sample data, one ignores the model uncertainty [28].

A. Building Robust Predictive Models through Bayesian Model Averaging

One possible approach to circumvent this problem is to weight all the possible models by their corresponding probability of being the true model, and use all of these in the experiment design step so that model uncertainty can be taken care of for Bayesian Optimization. In other words, the derived predictive model is a marginalized aggregation of all the potential predictive models, weighted by the prior probability and likelihood of the observed data for that model, resulting in the Bayesian Model Averaging (BMA) method [29, 30].

Here, we discuss the multi-output case from which the single output can be readily deduced. Let y^j represent the j^{th} output of interest, and \mathbf{x} the corresponding vector of features or materials design parameters, and the observed data be denoted by $\mathcal{D} = \{\mathbf{X}, \mathbf{Y}\}$, where $\mathbf{Y} = [Y^1, \dots, Y^q]$ is a matrix having the collection of the observed j^{th} output as its j^{th} column, i.e. $Y^j = [y_1^j, \dots, y_n^j]^T$, where n is the number of observed data points, and \mathbf{X} represent the matrix of the collection of the corresponding observed features. Here, to simplify the notation we have dropped the subscript denoting the experiment iteration step for \mathcal{D} , but note that $\mathcal{D} = \mathcal{D}_n$ at any n th step. The predictive probabilistic model for \mathbf{y} for a new feature vector \mathbf{x} after observing \mathcal{D} is

$$P(\mathbf{y}|\mathbf{x}, \mathcal{D}) = \sum_{i=1}^L P(M_i|\mathcal{D})P(\mathbf{y}|\mathbf{x}, \mathcal{D}, M_i), \quad (2)$$

where $P(\mathbf{y}|\mathbf{x}, \mathcal{D}, M_i)$ represents each potential prob-

abilistic predictive model, and

$$P(M_i|\mathcal{D}) = \frac{P(\mathcal{D}|M_i)P(M_i)}{\sum_{j=1}^L P(\mathcal{D}|M_j)P(M_j)}, \quad (3)$$

$$P(\mathcal{D}|M_i) = \int P(\mathcal{D}|\theta_i, M_i)P(\theta_i|M_i)d\theta_i, \quad (4)$$

are the (posterior) probability of each model being the true predictive model, and the marginal probability of the observed data under model M_i , respectively. L is the total number of models under consideration, and M_i and θ_i represents the i^{th} model and the vector of i^{th} model parameters, respectively.

If we further assume independence among outputs and let \mathcal{D}_j denote $\{\mathbf{X}, Y^j\}$, we have $P(\mathbf{y}|\mathbf{x}, \mathcal{D}, M_i) = \prod_{j=1}^q P(y^j|\mathbf{x}, \mathcal{D}_j, M_i)$ and

$$\begin{aligned} P(\mathcal{D}|M_i) &= \prod_{j=1}^q P(\mathcal{D}_j|M_i) \\ &= \prod_{j=1}^q \int P(\mathcal{D}_j|\theta_i^j, M_i)P(\theta_i^j|M_i)d\theta_i^j. \end{aligned} \quad (5)$$

When each potential probabilistic predictive model M_i is a Gaussian Process Regression (GPR) model [31], θ_i^j are the parameters of the covariance function. In fact, each GPR model M_i is defined by a mean (basis) function ($m_i^j(\cdot)$) and a covariance function ($K_i^j(\cdot, \cdot; \theta_i^j)$). In this setup, $P(y^j|\mathbf{x}, \mathcal{D}, M_i)$ is a Gaussian distribution, i.e. $P(y^j|\mathbf{x}, \mathcal{D}, M_i) = \mathcal{N}(\mu_i^j(\mathbf{x}), \sigma_i^{2,j}(\mathbf{x}))$, where the predicted mean and variance of the j^{th} objective function are [31]:

$$\begin{aligned} \mu_i^j(\mathbf{x}) &= m_i^j(\mathbf{x}) + K_i^j(\mathbf{x}, \mathbf{X}; \theta_i^j)K_i^j(\mathbf{X}, \mathbf{X}; \theta_i^j)^{-1}(Y^j - m_i^j(\mathbf{X})) \\ \sigma_i^{2,j}(\mathbf{x}) &= K_i^j(\mathbf{x}, \mathbf{x}; \theta_i^j) - K_i^j(\mathbf{x}, \mathbf{X}; \theta_i^j)K_i^j(\mathbf{X}, \mathbf{X}; \theta_i^j)^{-1}K_i^j(\mathbf{X}, \mathbf{x}; \theta_i^j). \end{aligned} \quad (6)$$

In practice, when using type II maximum likelihood (ML-II) estimation, the covariance function parameters of each model are estimated by maxi-

mizing the marginal log-likelihood of the observed data under that model, i.e. an estimate $\hat{\theta}_i^j$ is calculated by maximizing

$$\log P(\mathcal{D}_j|\hat{\theta}_i^j, M_i) = -\frac{1}{2}(Y^j - m_i^j(\mathbf{X}))^T K_i^j(\mathbf{X}, \mathbf{X}; \hat{\theta}_i^j)^{-1}(Y^j - m_i^j(\mathbf{X})) - \frac{1}{2}|K_i^j(\mathbf{X}, \mathbf{X}; \hat{\theta}_i^j)| - \frac{n}{2}\log 2\pi, \quad (7)$$

where $|\cdot|$ denotes matrix determinant. A quasi-

Newton method with multiple random starts can be

employed to find the maximum of (7). This estimate $\hat{\theta}_i^j$ is then used in (6) for prediction purposes under the model assumptions.

For a GPR, $P(\mathcal{D}_j|\theta_i^j, M_i)$ is a multivariate Gaussian probability density function, and $P(\mathcal{D}_j|M_i) = \int P(\mathcal{D}_j|\theta_i^j, M_i)P(\theta_i^j|M_i)d\theta_i^j$, the marginal probability of the observed data corresponding to j^{th} output under model M_i in (4), can be approximated by either first-order expansion of the exponent, or second-order expansion of the exponent known as Laplace approximation method [31]. In the first-order approximation, since $\hat{\theta}_i^j$ is a stationary point of (7), $P(\mathcal{D}_j|M_i)$ can be approximated by $P(\mathcal{D}_j|\hat{\theta}_i^j, M_i)$. In the second-order approximation, $P(\mathcal{D}_j|M_i) \approx P(\mathcal{D}_j|\hat{\theta}_i^j, M_i) \int \exp(-\frac{1}{2}(\theta_i^j - \hat{\theta}_i^j)^T(-H(\hat{\theta}_i^j))(\theta_i^j - \hat{\theta}_i^j))d\theta_i^j$, where $H(\hat{\theta}_i^j)$ is the Hessian matrix of $\log P(\mathcal{D}_j|\theta_i^j, M_i)$ calculated at $\hat{\theta}_i^j$. When all the models are assumed to have the same probability *a priori*, the posterior model probabilities in (3), i.e. $P(M_i|\mathcal{D}), i = 1, \dots, L$, are only dependent on the marginal probability of the observed data under each model in (4), i.e. $P(\mathcal{D}|M_i), i = 1, \dots, L$.

B. Experiment Design by Bayesian Optimization

Bayesian Experiment Design (BED) has the potential to guide efficient search for desired materials by directing sequential search of “optimal” query points to approach the optimal solution [11]. Here, we employ the Expected Improvement (EI) [10] for single objective problems, and an extension of EI to guide the search to approach the Pareto front for multi-objective problems, namely the Expected Hyper-Volume Improvement (EHVI) [32]. Both EI and EHVI can balance exploration and exploitation in guiding the search for optimal solutions.

A *major innovation* in our BED approach is that instead of assuming knowledge of the best predictive model in advance and updating this given predictive model based on the limited number of initial observed data and iterating the experiment design loop based on the updated model—an approach that is taken in the literature—we consider the model uncertainty by including a class of potential predictive models for the task under study. By BMA,

the experiment design step is performed based on the weighted average of these potential models. After performing the selected experiment, the new observed data from the experiment is used to update the (posterior) probability of all these potential predictive models. We can see that by taking this approach, as more experiments are done, the true predictive model is selected with a higher probability alongside accelerating the discovery of the material with the desired properties.

For the special case of employing EI-based BED [10], the EI after observing data \mathcal{D} can be computed under model averaging by:

$$\begin{aligned} EI(\mathbf{x}|\mathcal{D}) &= E[I(y|\mathbf{x})|\mathcal{D}] = \int I(y|\mathbf{x}, \mathcal{D})P(y|\mathbf{x}, \mathcal{D})dy \\ &= \int I(y|\mathbf{x}, \mathcal{D}) \sum_{i=1}^L P(M_i|\mathcal{D})P(y|\mathbf{x}, \mathcal{D}, M_i)dy \\ &= \sum_{i=1}^L P(M_i|\mathcal{D}) \int I(y|\mathbf{x}, \mathcal{D})P(y|\mathbf{x}, \mathcal{D}, M_i)dy \\ &= \sum_{i=1}^L P(M_i|\mathcal{D})EI(\mathbf{x}|\mathcal{D}, M_i), \end{aligned} \tag{8}$$

where $I(y|\mathbf{x}, \mathcal{D})$ denotes the improvement achieved by observing the output of experiment \mathbf{x} , E represents expectation, and $EI(\mathbf{x}|\mathcal{D}, M_i)$ is the EI under model M_i . In this approach, the optimal experiment to be performed next is $\mathbf{x}^* = \underset{\mathbf{x} \in \mathcal{X}}{\text{argmax}} EI(\mathbf{x}|\mathcal{D})$.

We can see that the optimal experiment is the one that maximizes the weighted average EI considering all the potential predictive models based on the iteratively updated (posterior) model probabilities given the observed data. In the equations above, the improvement achieved by observing the output of experiment \mathbf{x} is $I(y|\mathbf{x}, \mathcal{D}) = (y^* - y)_+$ when minimization is the goal, and $I(y|\mathbf{x}, \mathcal{D}) = (y - y^*)_+$ when maximization is the goal, where $(a)_+ = a$ if $a > 0$ and is zero otherwise, and y^* denotes the best (lowest/highest for minimization/maximization problems) output observed so far, i.e. the best output in \mathcal{D} .

Similarly, for multi-objective problems, the EHVI under model averaging is

$$\begin{aligned}
EI_{\mathcal{H}}(\mathbf{x}|\mathcal{D}) &= E[I_{\mathcal{H}}(\mathbf{y}|\mathbf{x})|\mathcal{D}] = \int I_{\mathcal{H}}(\mathbf{y}|\mathbf{x}, \mathcal{D})P(\mathbf{y}|\mathbf{x}, \mathcal{D})d\mathbf{y} = \int I_{\mathcal{H}}(\mathbf{y}|\mathbf{x}, \mathcal{D}) \sum_{i=1}^L P(M_i|\mathcal{D})P(\mathbf{y}|\mathbf{x}, \mathcal{D}, M_i)d\mathbf{y} \\
&= \sum_{i=1}^L P(M_i|\mathcal{D}) \int I_{\mathcal{H}}(\mathbf{y}|\mathbf{x}, \mathcal{D})P(\mathbf{y}|\mathbf{x}, \mathcal{D}, M_i)d\mathbf{y} = \sum_{i=1}^L P(M_i|\mathcal{D})EI_{\mathcal{H}}(\mathbf{x}|\mathcal{D}, M_i),
\end{aligned} \tag{9}$$

where $I_{\mathcal{H}}(\mathbf{y}|\mathbf{x}, \mathcal{D})$ denotes the hyper-volume improvement achieved by observing the outputs at \mathbf{x} , and $EI_{\mathcal{H}}(\mathbf{x}|\mathcal{D}, M_i)$ is the ordinary EHVI under model M_i . If the outputs are assumed to be independent $EI_{\mathcal{H}}(\mathbf{x}|\mathcal{D}, M_i)$ further simplifies to $\int I_{\mathcal{H}}(\mathbf{y}|\mathbf{x}, \mathcal{D}) \prod_{j=1}^q P(y^j|\mathbf{x}, \mathcal{D}, M_i)d\mathbf{y}$. The optimal experiment to be performed next is $\mathbf{x}^* = \underset{\mathbf{x} \in \mathcal{X}}{\operatorname{argmax}} EI(\mathbf{x}|\mathcal{D})$, which is the one that

maximizes the weighted average EHVI considering all the potential predictive models, again by the iteratively updated (posterior) model probabilities. The hyper-volume improvement $I_{\mathcal{H}}(\mathbf{y}|\mathbf{x}, \mathcal{D})$ is the increase in the hyper-volume of the dominated (objective) space achieved by adding the outputs at \mathbf{x} to the observed data, i.e. $I_{\mathcal{H}}(\mathbf{y}|\mathbf{x}, \mathcal{D}) = \mathcal{H}(\mathbf{Y} \cup \mathbf{y}) - \mathcal{H}(\mathbf{Y})$. Without loss of generality, if we assume the goal is minimization of all the outputs, the hyper-volume dominated by a set of points \mathbf{A} is defined as the volume of the dominated subspace by the points in \mathbf{A} , i.e. $\mathcal{H}(\mathbf{A}) = \operatorname{Volume}(\{\mathbf{s} \in \mathbb{R}^q | \mathbf{s} \prec \mathbf{r} \text{ and } \exists \mathbf{a} \in \mathbf{A} : \mathbf{a} \prec \mathbf{s}\})$, where the domination rule is such that $\mathbf{a} \prec \mathbf{b}$ if and only if $a^j \leq b^j$ for all $j = 1, \dots, q$, and for at least one j , $a^j < b^j$. \mathbf{r} is called a reference or anchor point and is a point dominated by all the possible output values (the whole output space).

For the GPR model assumptions taken by the experiments in this paper, we have chosen the constant mean function (i.e. $m_i(\mathbf{x}) = c_i$ for single output and $m_i^j(\mathbf{x}) = c_i^j$ for multiple output cases) and the (Gaussian) Radial Basis Function (RBF) kernel, a popular choice, for the covariance function:

$$K_i^j(\mathbf{x}, \mathbf{x}'; \theta_i^j) = \theta_{i,1}^j \exp\left[-\frac{1}{2} \frac{\|\mathbf{x} - \mathbf{x}'\|^2}{\theta_{i,2}^j}\right]. \tag{10}$$

The focus of the experiments in this paper is on showing the power of experiment design considering model uncertainty by BMA in guiding the search towards the optimal compound (with corresponding features design parameters) when the best predictive model is not known in advance, a usual case in practical applications, while also identifying the best predictive model as more data from experi-

ments become available. The algorithm for our proposed Bayesian Optimization under Model Uncertainty (BOMU) framework is shown in Algorithm 2 and the overall framework for autonomous materials discovery is shown in Fig. 2.

In this paper we consider predictive models based on different potential feature sets. The details are provided in the following section.

Algorithm 2 Bayesian Optimization under Model Uncertainty

- 1: Initialize \mathcal{D}_0
- 2: **for** $n=0, 1, \dots$ **do**
- 3: Compute acquisition function u with model averaging:

$$u = EI(\mathbf{x}|\mathcal{D}_n) = \sum_{i=1}^L P(M_i|\mathcal{D}_n)EI(\mathbf{x}|\mathcal{D}_n, M_i)$$

- 4: Select new \mathbf{x}_{n+1} by optimizing acquisition function u :

$$\mathbf{x}_{n+1} = \underset{\mathbf{x} \in \mathcal{X}}{\operatorname{argmax}} u(\mathbf{x}; \mathcal{D}_n)$$

- 5: Query blackbox function f to obtain y_{n+1}
 - 6: Augment data $\mathcal{D}_{n+1} = \{\mathcal{D}_n, (\mathbf{x}_{n+1}, y_{n+1})\}$
 - 7: Update statistical model(s), M_i
 - 8: **end for**
-

III. DEPLOYMENT OF BOMU: OPTIMAL DISCOVERY OF THE MAX PHASE SPACE

$M_{n+1}AX_n$ phases— M corresponds to a transition metal, A corresponds to group IV and VA elements, and X corresponds to carbon or nitrogen—have a property range within those of ceramics and metals due to the coexistence of both metallic and metallic/covalent bonds within their layered structures [18, 33–37]. The bonds between M-A layers tend to be much weaker than those between M-X layers, making them easily deformable while retaining much of the chemical (and thermodynamic) stability of transition MX carbides. While only a very small fraction of the pure ternary MAX phase composition palette has been synthesized to

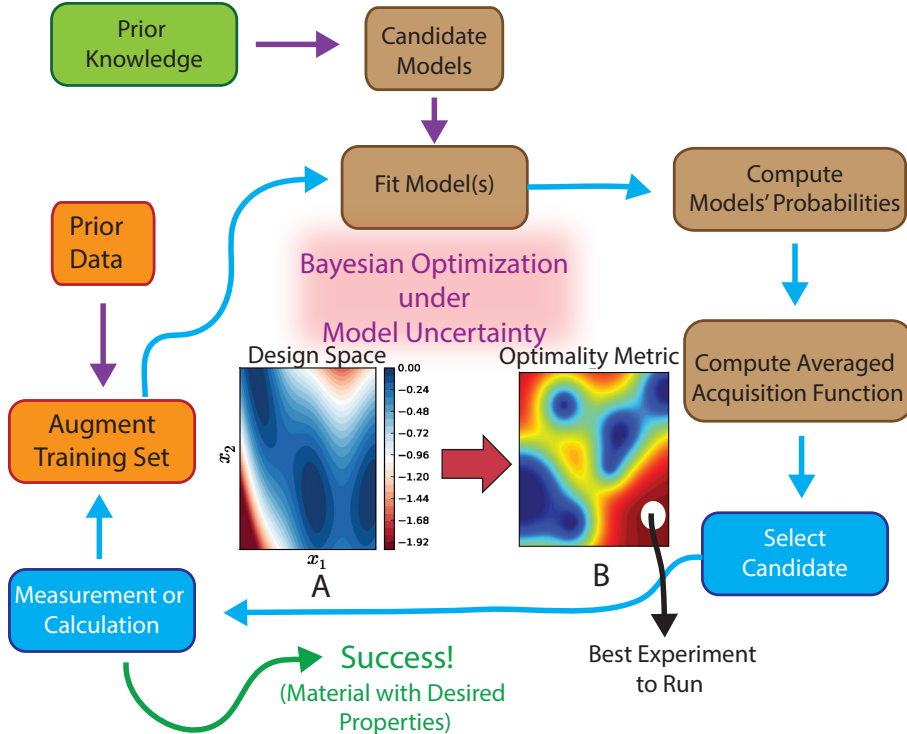


FIG. 2: Schematic of the proposed framework for an autonomous, efficient materials discovery system as a realization of Bayesian Optimization under Model Uncertainty (BOMU). Initial data and a set of candidate models are used to construct a stochastic representation of an experiment/simulation. Each model is evaluated in a Bayesian sense and its probability is determined. Using the model probabilities, an effective acquisition function is computed, which is then used to select the next point in the materials design space that needs to be queried. The process is continued iteratively until target is reached or budget is exhausted.

date [38], there is a considerable opportunity to uncover promising chemistries with optimal property sets once different stacking sequences and deviations from stoichiometries in the M, A, and X sites are considered [39, 40].

A. Design Problem: Optimal Mechanical Properties in the MAX Phase Space

Because of their rich chemistry and the wide range of values of their properties [41], MAX phases constitute an adequate material system to test simulation-driven—specifically DFT calculations—materials discovery frameworks. Aryal *et al.* [41], for example, carried out an exhaustive investigation of the structural, electronic and stability properties of 792 MAX phases with the $M_{n+1}AX_n$ and $n = 1-4$. Balachandran *et al.* [17] used the MAX phases with M_2AX stoichiometry to deploy and test differ-

ent Bayesian Optimization schemes. In this work, we use the same system to test the proposed framework.

The MDS for this work is composed of conventional MAX phases with M_2AX and M_3AX_2 stoichiometries. Here $M \in \{Sc, Ti, V, Cr, Zr, Nb, Mo, Hf, Ta\}$; $A \in \{Al, Si, P, S, Ga, Ge, As, Cd, In, Sn, Tl, Pb\}$; and $X \in \{C, N\}$. This results in 216 M_2AX and 216 M_3AX_2 phases. Since we are testing a materials discovery framework, we found it convenient to determine the ground truth of the system beforehand and the mechanical properties of these systems were thus determined before deploying the BOMU framework—our framework has been incorporated into a high-throughput workflow automation tool using the scikit-learn [42] toolbox. The implementation is publicly available at <https://gitlab.com/tammal/matpredict>. Of the possible MAX phases with the chemistries described

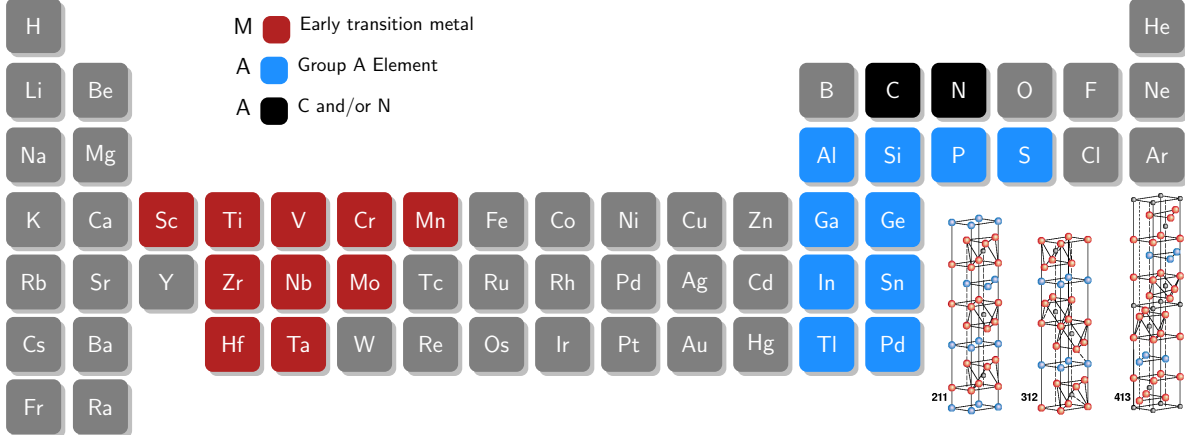


FIG. 3: MAX Phases: ternary (and higher order) layered carbides and nitrides with properties intermediate to those of metals and ceramics [18].

above, 29 were found to be elastically unstable and were discarded. The design space thus consists of 403 MAX phases.

The problem was formulated with the goal of identifying the material/materials with i) the maximum bulk modulus K ; ii) the minimum shear modulus G ; and iii) the maximum bulk modulus and minimum shear modulus. The cases of i) the maximum bulk modulus K ; ii) the minimum shear modulus G are designed as single-objective optimization problems. The third problem which seeks to identify the materials with the maximum bulk modulus and minimum shear modulus (iii) is designed as a multi-objective problem.

B. Prior Knowledge

In this framework, it is assumed that some prior knowledge is available before starting the materials discovery task. This prior knowledge could be as simple as a set of features that are likely to have effects on the materials properties of interest. Here we describe the features that were selected to constitute the MDS:

Each candidate MAX phase c_i of the MDS is determined uniquely by a set of features F_j , which have been distilled from the existing literature and the authors' domain knowledge. In the MDS, the M & A chemical elements comprising the MAX phases sweep along the rows and columns of the periodic table and it is reasonable to expect that features which intrinsically reflect periodic trends would characterize the properties of the MAX phases.

In this work, a total of fifteen features were considered: empirical constants C, m which relate the elements comprising the material to its bulk modulus [43]; valence electron concentration C_v ; electron to atom ratio $\frac{e}{a}$; lattice parameters a and c ; atomic number Z ; interatomic distance I_{dist} ; the groups according to the periodic table of the M, A & X elements Col_M, Col_A, Col_X respectively; the order O of MAX phase (whether of order 1 corresponding to M_2AX or order 2 corresponding to M_3AX_2); the atomic packing factor APF ; average atomic radius rad ; and the volume/atom vol . In relevant cases ($C, m, C_v, \frac{e}{a}, Z, I_{dist}, APF, C_v$), these features are composition-weighted averages calculated from the elemental values and are assumed to propagate as per the Hume-Rothery rules.

The C, m parameters are related to the bonding character. These are composition-weighted values of the empirical constants reported by Makino *et al.*[43], who proposed that the bulk modulus \mathbf{K} of elemental substances can be determined by the relation $K = Cr_{ps}^{-m}$; where r_{ps} is the effective pseudopotential radius. The valence electron concentration C_v is another feature related to the bonding character and is a known marker of the stability of a phase [44, 45]. The $\frac{e}{a}$ ratio, which is the average number of itinerant electrons per atom, plays a significant role in the bonding of a solid and is closely related to the valence electron concentration C_v [46].

The lattice parameters c, a for all the domain elements were calculated by DFT by allowing the structures to completely relax. The c lattice parameter is highly correlated to the order of the MAX phase (whether M_2AX or M_3AX_2). The lattice parameters implicitly account for the effect of volume and

atomic radius on the elastic properties. Additionally, the c/a ratio characterizes the MAX phases, they being hexagonal close packed (hcp) materials. The relationship between the elastic properties and the c/a ratio for hcp materials has also been extensively studied [47, 48]. Here we note that since the determination of the equilibrium structural parameters is approximately an order of magnitude less costly than full calculation of the elastic constant tensor and thus it is a reasonable proposition to use these DFT-derived quantities to assist in the prediction/discovery of properties that are more costly to acquire.

The atomic number Z , which denotes the number of electrons is the foremost factor that determines the chemical bonding behavior of a material and defines its chemical properties. The weighted interatomic distance I_{dist} was calculated from the elemental values, which were sourced from the CRC Handbook of Chemistry and Physics [49]. The atomic packing factor (APF) plays an important role in the determination of elastic properties. For example, face centered cubic (fcc) structures tend to be ductile, while hcp structures are brittle. Finally, the structural parameters: average atomic radius rad and the volume/atom vol were determined from the DFT-determined lattice parameters.

C. Determining Candidate Models/Theories

As discussed, the determination of features comprising the MDS was based off of prior literature and domain knowledge. *A priori*, it is not known which of these features significantly influence the target properties in the materials discovery task. In the search for new materials with desired properties, such situations are often encountered, where there is a lack of fundamental knowledge relating the intrinsic nature of the material and the desired property. The BOMU approach invoked in this work accounts for uncertainty in the models M_i available to fit the blackbox predictive model to observed data. In our design problem, different models M_i correspond to different subsets \mathcal{F}_S out of the entire feature set \mathcal{F} , $\mathcal{F}_S \subseteq \mathcal{F}$.

While one could question the need to define candidate feature subsets \mathcal{F}_S when the entire feature set \mathcal{F} is available, it is important to note that exploring the entire feature set is problematic due to important limitations [50]. First, non-parametric regression is challenging in high-dimensional space, with lower bounds of nearest-neighbour distance between samples depending exponentially on the dimension

TABLE I: Feature Sets Considered in this Design

F_1	$[C, m, C_v, c]$
F_2	$[m, Z, I_{dist}, \frac{c}{a}]$
F_3	$[\frac{c}{a}, a, c, C_v]$
F_4	$[C, m, C_v, Col_A]$
F_5	$[Col_M, Col_A, Col_X, O]$
F_6	$[a, c, APF, I_{dist}]$

of the problem [51]. This exponential complexity affects the convergence rate of BO approaches [52]. Second, the computational effort in maximizing the acquisition function also increases in an exponential manner with the number of features.

The general problem of Bayesian Optimization in the presence of many potential models (feature sets) is still an outstanding challenge [53] and different approaches have been proposed, including the partitioning of the domain in disjoint subdomains [50] or the use of random embedding [53]. No approach so far provides the means for the BO framework itself to ‘learn’ the optimal model and select the subspace most effectively to reach the target property(ies). Our proposed approach, as will be shown below, **addresses these issues** and thus constitutes a novel approach to effectively reduce the complexity of the BO problem under model uncertainty.

D. Selecting Feature Sets

Feature selection is an essential component of model construction and learning and is a research area in itself. Application of rigorous feature selection methods can lead to better models with a good understanding of the underlying characteristics of the data. Using the right features reduces the complexity of the model and reduces overfitting. Choosing the right subset of features also improves the accuracy of a model. For the purposes of this work, we elected to see how far one can get by choosing to rely on simpler methods. To reduce the feature space dimensionality of the model, we grouped the features into 6 sets containing 4 features each, as shown in Table I.

These sets were created *ad hoc*, using a combination of physical insights and an effort to make sets containing features which reflect the effect of electronic structure and chemical bonding character. For example, since C and m are derived from Makino’s empirical model [43], they were grouped together in sets F_1 and F_4 . In set F_2 , m was used standalone, since the empirical relationship

$K = Cr_{ps}^{-m}$ indicates that m is more significant than C , which only introduces the effect of a constant. In set F_5 , only the compositional element markers (Col_M, Col_A, Col_X) along with the order O of MAX phase were used, to simulate a feature set which has only the most basic compositional and structural description.

A Pearson correlation matrix [54] was calculated for all the features and is shown in Fig.4. A Pearson coefficient ρ , is a linear correlation measure between two features f_1 and f_2 and may be calculated as:

$$\rho_{f_1, f_2} = \frac{cov(f_1, f_2)}{\sigma_{f_1} \sigma_{f_2}}, \quad (11)$$

where cov denotes the covariance, σ_{f_1} is the standard deviation of f_1 , and σ_{f_2} is the standard deviation of f_2 . The value of the coefficient lies in $[-1, 1]$, with 1 indicating perfect positive linear correlation and -1 indicating perfect negative linear correlation. The goal is to get the best results possible by using the minimum number of features. Ideally, the feature pairs should be uncorrelated, which will ensure that we are not needlessly increasing the dimensionality of the feature space without substantially improving the results. Highly correlated features can be redundant and are undesirable, since they will increase the dimensionality of the feature space without proportionally increasing the information available to optimize the objective function.

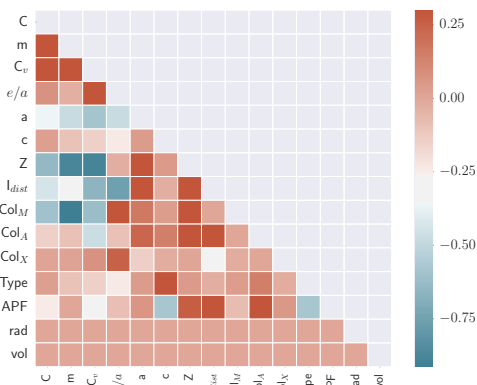


FIG. 4: Pearson correlation matrix for the features used in this work. Small (lighter) values correspond to feature pairs with little correlation between them.

E. Materials Discovery/Design Protocol

GPR models based on six feature subsets in Table I, were adopted in our BMA experiment design. For each of the targets (maximizing K, minimizing G, as well as maximizing-K/minimizing G) we carried out the sequential experiment design by maximizing the EI or EHVI based on predictive models using single feature sets or BMA using all the feature sets accounting for their probability through first-order (BMA₁) and second-order (BMA₂) Laplace approximation.

The optimization scheme was run for initial data sets (i.e known data points) of size $N = 2, 5, 10, 15, 20$. The ‘training set’ thus ranges from $\approx 1/200$ to $1/20$ of the MDS. 1500 instances of each initial set N were used to ensure a stable average response. The budget for the optimal design was set at $\approx 20\%$ of the MDS, i.e 80 materials or calculations. In each iteration, two calculations were done. This means that for example, for the maximization of the bulk modulus problem for $N=2$, we initially know the bulk modulus of 2 materials ($N=2$) and can calculate the bulk modulus of 78 more materials to stay within the budgeted 80 calculations. Since we are calculating the bulk modulus of 2 materials at a time, this means a total of $78/2 = 39$ iterations for this case. All the input features were normalized, before being fed to the optimization module.

F. DFT Calculation Parameters

The total energy calculations were performed within the DFT [55] framework, as implemented in the *Vienna ab initio* simulation package (VASP) [56, 57]. The generalized gradient approximation (GGA) [58] is used in the form of the parameterization proposed by Perdew, Burke, and Ernzerhof (PBE) [59, 60]. Brillouin zone integrations were performed using a Monkhorst-Pack mesh [61] with at least 5000 k points per reciprocal atom. Full relaxations were realized by using the Methfessel-Paxton smearing method [62] of order one and a final self-consistent static calculation with the tetrahedron smearing method with Blöchl corrections [63]. A cutoff energy of 533 eV was set for all of the calculations and the spin polarizations were taken into account.

To estimate the lattice parameters, the structures were allowed to fully relax to their ground states. The relaxations were carried out in six stages: first stage by allowing change in volume (corresponding

to the VASP ISIF =7 tag), second stage by additionally allowing the relaxation of cell shape (corresponding to the VASP ISIF =6 tag), third stage by also allowing relaxation of ions (corresponding to the VASP ISIF =3 tag), fourth stage by allowing only the ions to relax (corresponding to the VASP ISIF =2 tag), fifth stage by allowing full relaxation (VASP ISIF =3 tag) and a final self-consistent static calculation run. All relaxations were carried out until changes in total energy between relaxation steps were within 1×10^{-6} eV.

The elastic constants were calculated using the stress-strain approach [64, 65] where a set of strains ($\epsilon_1; \epsilon_2; \epsilon_3; \epsilon_4; \epsilon_5; \epsilon_6$) were imposed on a crystal, determined using DFT methods as described in [66]. From the n set of strains and the resulting stresses, elastic constants were calculated based on Hooke’s law. For these calculations, the ionic positions were relaxed while leaving the lattice shape and volume invariant. These calculations were followed by a static calculation using order-one Methfessel-Paxton smearing method and an auxiliary FFT grid to ensure maximum accuracy in the calculation of interatomic forces. Convergence criteria ensured that calculated elements of elastic constant tensor changed within a few GPa when varying the magnitude of the lattice strain from 1% to 3%. From these elastic constants, various elastic properties have been calculated using the Voigt and Reuss approximations and Voigt-Reuss-Hill averaging [67]. The properties under consideration are: the bulk modulus (K) and the shear Modulus (G).

IV. RESULTS

As mentioned earlier, we employ the EI and EHVI acquisition functions in the experiment design loop for single and multi-objective problems, respectively. Hereafter, a single model is a Gaussian Process Regression (GPR) model based on a single feature set. Also, $F_1, F_2, F_3, F_4, F_5,$ and F_6 denote the 6 different feature sets considered in our analysis, the GPR models based on those feature sets, and experiment design assuming the underlying model based on those feature sets, interchangeably. In the following “convergence” for each model (feature set) refers to the calculation number in the experiment design iterations based on that model (feature set) when the true optimal design parameters are identified in (nearly) all simulations with 1500 initial data sets with different size N for each setup.

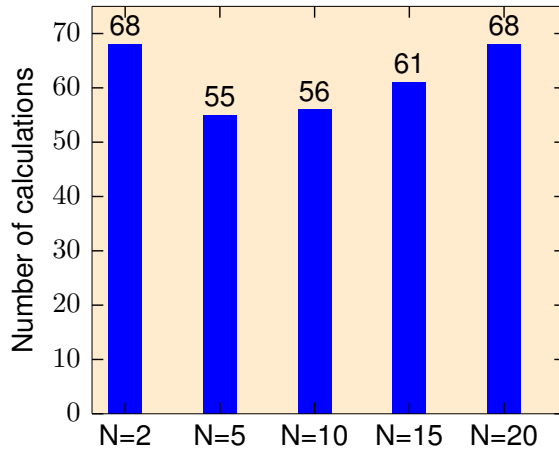


FIG. 5: Average number of calculations required to find maximum bulk modulus for different numbers of initial data instances $N = 2, 5, 10, 15, 20$ using feature set F_2

A. Single objective optimization

1. Maximization of bulk modulus (K)

As mentioned earlier, calculations were carried out for different number of initial data instances $N = 2, 5, 10, 15, 20$. The performance trends for all three problems across different values of N are consistent. The technique is found to not significantly depend on quantity of initial data. Fig. 5 shows the average number of calculations required to find maximum bulk modulus for $N = 2, 5, 10, 15, 20$ with F_2 . Even when we start with very few initial data instances at $N = 2$, the Bayesian experiment design (BED) procedure converges at least as fast as $N = 20$. Using $N = 5$ however, leads to faster convergence than starting with $N = 10, 15, 20$. This shows that it is often more effective to start with a small initial data set. This is advantageous, since in real-world problems, scarcity of data is a common limitation. Consequently, for the sake of brevity, we present results using the representative case of $N = 10$ only. Results for $N = 2, 5, 15, 20$ may be found in the Supplementary figures.

For the first test problem to find the MAX phase with the maximum bulk modulus, the maximum values found in the experiment design iterations based on each model (feature set) averaged over all initial data set instances for $N = 10$ are shown in Fig. 6a. The dotted line in the figure indicates the maximum bulk modulus = 300 GPa that can be found in the

MDS. F_2 is found to be the best performing feature set on average, converging fastest to the maximum bulk modulus. In other words, using the predicted values as well as uncertainty estimation from the GPR model with F_2 in the experiment design loop guides us toward the optimal solution of the problem faster than the other models. F_6 and F_5 on the other hand, are uniformly the worst performing feature sets on average, converging the slowest.

Fig. 6b shows the swarm plots indicating the number of calculations required to discover the maximum bulk modulus in the MDS using experiment design based on single models for the 1500 initial data instances with $N = 10$. The width of the swarm plot at every vertical axis value indicates the proportion of instances where the optimal design parameters were found at that number of calculations. The dotted line indicates the budget allotted, which was 80 calculations. Instances that did not converge within the budget were allotted a value of 100. Thus the width of the plots at vertical value of 100, corresponds to the proportion of instances which did not discover the maximum bulk modulus in the MDS within the budget. From this figure, it is seen that for F_1, F_2 and F_4 in almost 100 % of instances the maximum bulk modulus was identified within the budget, while F_5 is the poorest feature set and the maximum was identified in very few instances.

Fig. 6c shows the comparison of the average performance of both the first-order and second-order BMA over all initial data set instances with the best performing model (F_2) and worst performing model (F_6). It can be seen that both the first-order and second-order BMA performance in identifying the maximum bulk modulus is consistently close to the best model (F_2). First-order BMA performs as well as if not better than F_2 . Fig. 6d shows the corresponding swarm plots indicating the number of calculations required to discover the maximum bulk modulus in the MDS for the 1500 instances of initial data set for $N = 10$ using first- and second-order BMA, respectively. It can be seen that for a very high percentage of cases the maximum bulk modulus can be found within the designated budget.

In Figs. 7a and 7b, the average model coefficients (posterior model probabilities) of the GPR models based on different feature sets over all instances of initial data set are shown with the increasing number of calculations for BMA_1 and BMA_2 , respectively. It can be seen that these model coefficients from BMA may guide automatic selection of the best feature set F_2 . For BMA_1 and BMA_2 , the average probability of F_2 is (almost) always higher than the other models. Earlier, in Figs. 6a and 6b, F_4 also appears to be

a good model and converges at par with F_2 around the 75 calculations. Reflecting this, as the number of available experiments/calculations increases (55 for BMA_1 and 75 for BMA_2), the model probability of F_4 briefly overtakes that of F_2 as indicated in Fig. 7. As more data become available, BMA again considers F_2 as the best model based on the updated model coefficients during the experiment design procedure. Note that such a feature set selection based on BMA is directly determined by the performance of achieving desired operational objectives for experiment design.

The actual candidate materials selected during each progressive BED iteration with BMA_1 were analyzed over the 1500 instances, among which the cumulative percentage of choosing candidates with the maximum (K_{max}^1), second maximum (K_{max}^2), third maximum (K_{max}^3) bulk modulus is indicated in Fig. 8. It is seen that as the BED loop proceeds and the surrogate model improves, the materials with the maximum bulk modulus (top 3 for illustration) are selected more consistently. Specifically, beyond approximately 40 calculations, there is a steep increase in the selection of K_{max}^i as a candidate, corresponding to the steep increase in the probability of model F_4 and F_2 as illustrated in Fig. 7a.

2. Minimization of shear modulus (G)

Similar to maximization of bulk modulus, the optimization for the minimization problem was carried out for feature sets F_1, \dots, F_6 , and then by using BMA_1 and BMA_2 . The overall trend in the results was also similar: F_2 is found to be the best performing model on average, converging fastest to the minimum shear modulus. On the other hand, F_6 is uniformly the worst performing feature set on average, converging the slowest. The minimum shear modulus found in the experiment design iterations based on the best model (F_2), worst model (F_6), BMA_1 , and BMA_2 averaged over all initial data instances are shown in Fig. 9a for $N = 10$. The dotted line in the figure indicates the minimum shear modulus = 10.38 GPa that can be found in the MDS. The performance of both first-order and second-order BMA in identifying the minimum shear modulus lies close to that of the best single model (F_2). Fig. 9b shows the swarm plots corresponding to the results in Fig. 9a. It is seen that in almost 100 % of the cases the optimal solution (minimum shear modulus) can be found within the designated budget when feature set F_2 is used, while very few instances of convergence are noted for F_6 . Using BMA_1 and BMA_2

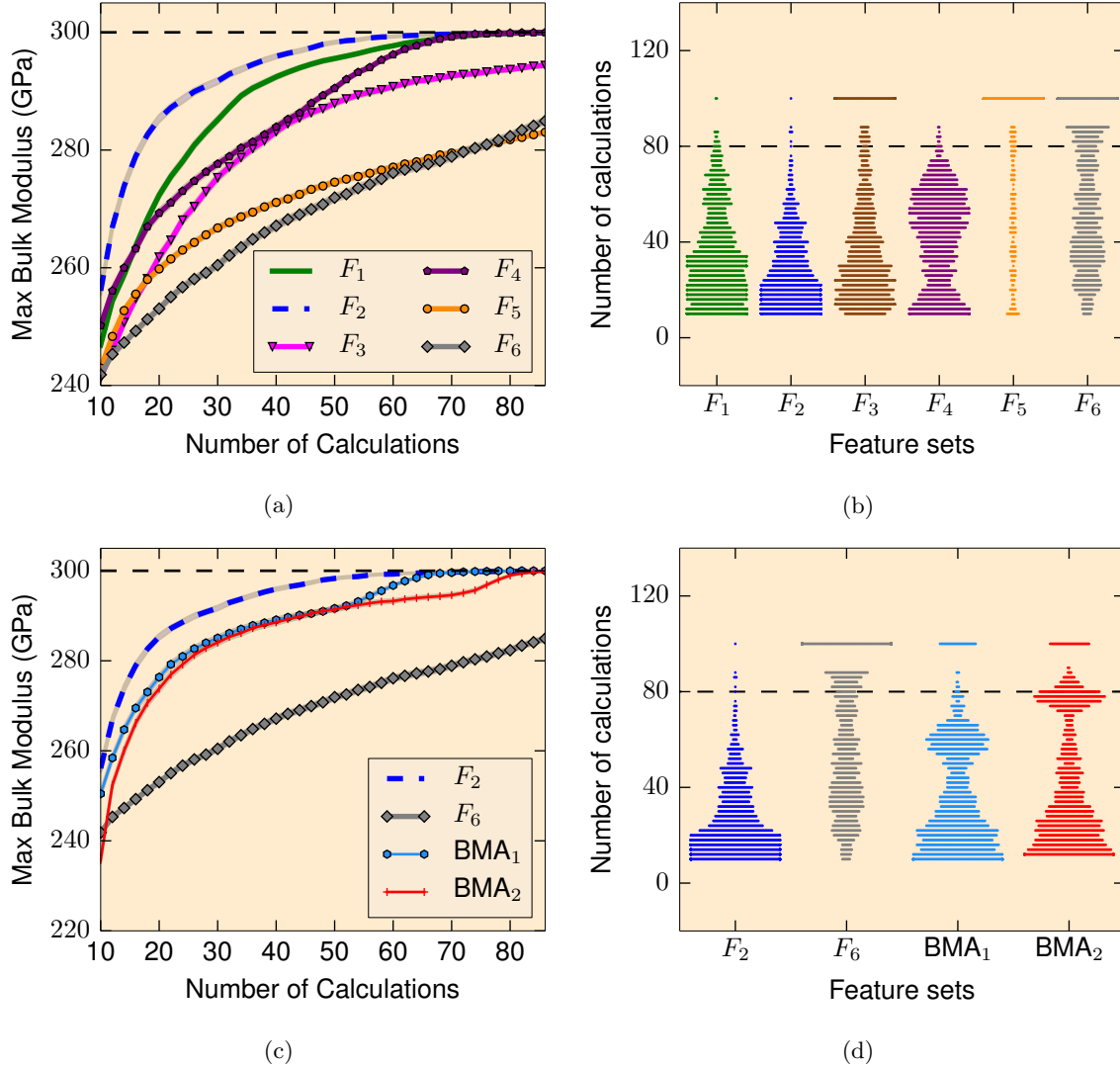


FIG. 6: Representative results for single objective optimization – maximization of bulk modulus for $N=10$: a) Average maximum bulk modulus discovered using all described feature sets, b) swarm plots indicating the distribution of the number of calculations required for convergence using all described feature sets, c) average maximum bulk modulus discovered using the best feature set F_2 , worst feature set F_6 , BMA₁ and BMA₂, and d) swarm plots indicating the distribution of the number of calculations required for convergence using best feature set F_2 , worst feature set F_6 , BMA₁ and BMA₂.

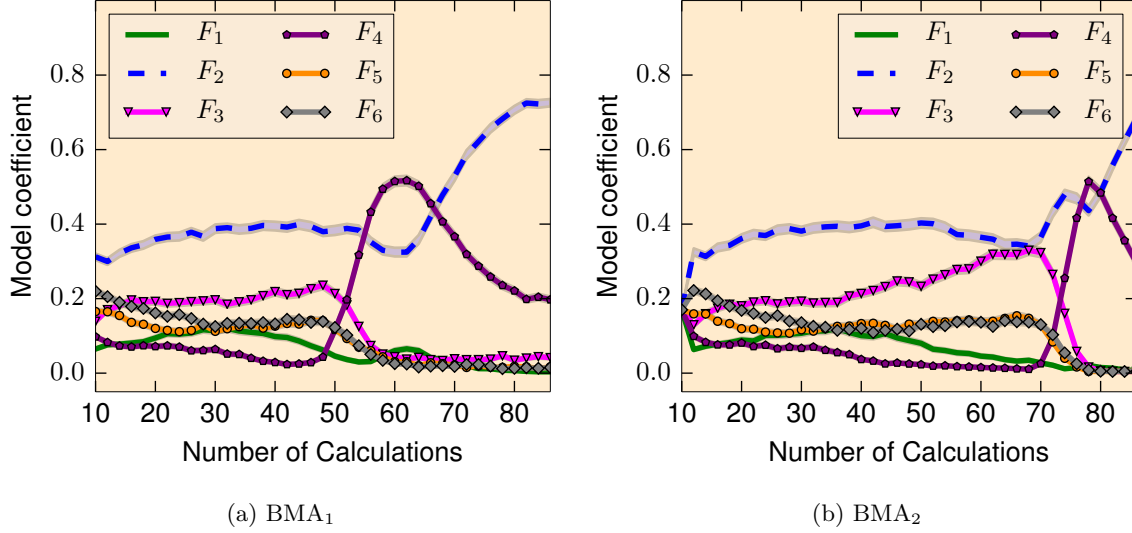


FIG. 7: Average model probabilities for maximizing bulk modulus using a) BMA₁ and b) BMA₂

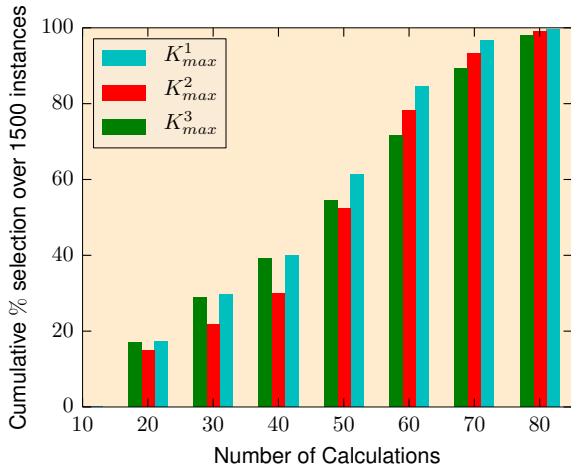


FIG. 8: Percentage of BED selected materials with the maximum (K_{max}^1), second maximum (K_{max}^2), third maximum (K_{max}^3) bulk modulus with the increasing number of calculations for BMA₁.

yields very satisfactory results, as a large majority of the cases converge within budget. Here, we see the advantage of using the BMA approach. Without having actually gone through the EGO loop, one could not know *a priori*, that using F_6 will result in not arriving at the desired material within a reasonable budget with a very high probability. This shows that if one were to just select a feature set even using domain knowledge, one may or may not

select a good model. However, if one were to use the BMA approach, either BMA₁ or BMA₂, the probability of successfully arriving at the material with desired properties, is very high, since the BMA approach auto-selects the best feature set. Results for $N = 2, 5, 15, 20$ as well as the plots for BMA coefficients may be found in the Supplementary figures.

B. Multi-objective optimization

1. Maximize bulk modulus and Minimize shear modulus

We now consider multi-objective experiment design to optimize two objectives at the same time: maximizing bulk modulus and minimizing shear modulus. One should note that in our analysis we have already calculated the responses of bulk and shear modulus as materials properties for all the feasible points in the MDS to have the ground truth to compare different models for experiment design. Generally in practice, no knowledge of the responses exists unless one performs all the possible experiments exhaustively. Consequently, none of this information is used in our experiment design procedures. Fig. 10 illustrates all the data points in the objective space of materials properties (in green). It can be seen that in this case there does not exist a single optimal solution, and in fact there are 10 *Pareto* optimal points comprising the *Pareto front*[68] which is highlighted in red in the

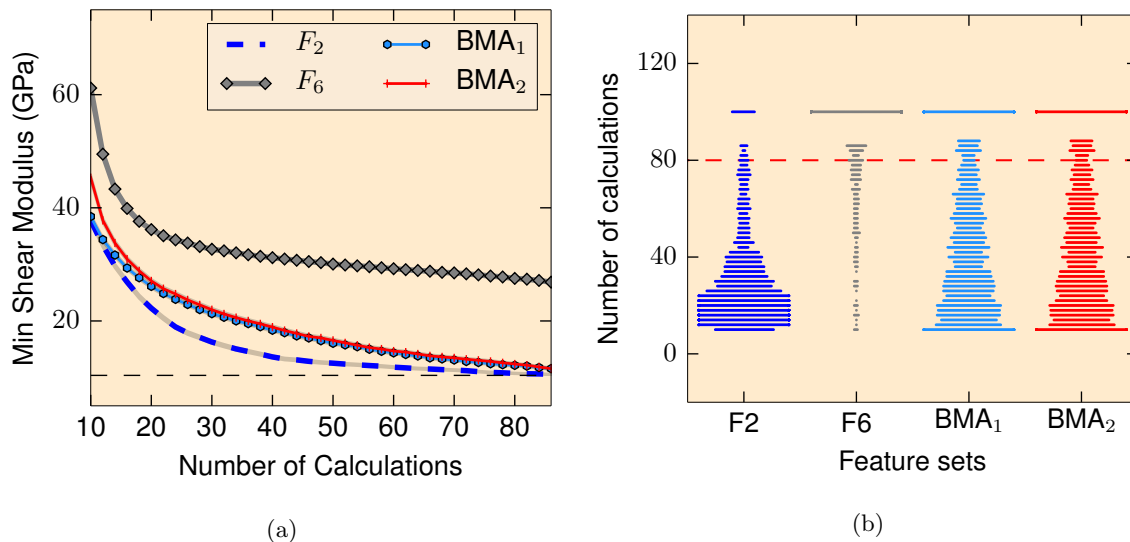


FIG. 9: Representative results for single objective optimization – minimization of shear modulus for $N=10$: a) average minimum shear modulus discovered using the best feature set F_2 , worst feature set F_6 , BMA_1 and BMA_2 , and d) swarm plots indicating the distribution of the number of calculations required for convergence using best feature set F_2 , worst feature set F_6 , BMA_1 and BMA_2 .

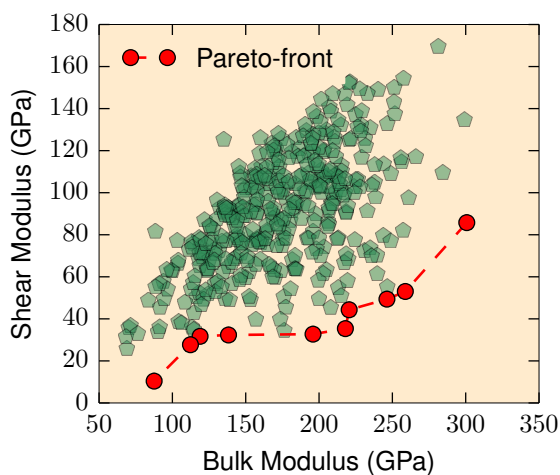


FIG. 10: The Pareto optimal points in the materials property space are marked in red corresponding to the criterion of maximizing bulk modulus and minimizing shear modulus simultaneously. The Pareto set for the MDS consist of 10 points as indicated in red.

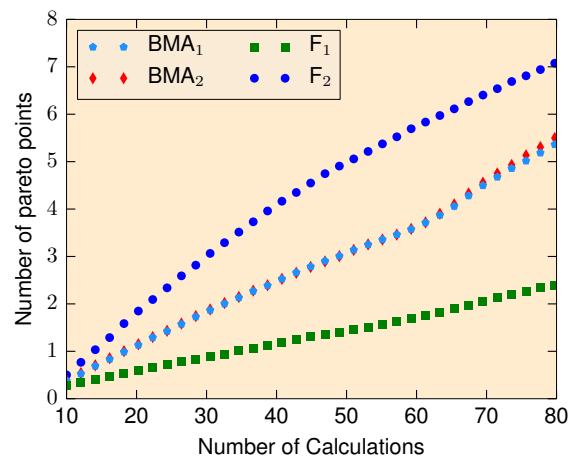


FIG. 11: Average number of true Pareto optimal points found over all initial data set instances for single models, BMA_1 , and BMA_2 for $N=10$

figure. Specifically, the *Pareto front* here is the 2-dimensional design surface over which any improvement in one material property (i.e bulk modulus K)

is only achieved through a corresponding sacrifice of another property (here, shear modulus G).

Fig. 11 depicts the average performance of the best (F_2) and worst (F_1) models as well as the first- and second-order BMA in finding the true Pareto optimal points versus the number of calculations. Similar to single-objective problems, multi-objective

experiment design based on F_2 consistently has the best performance; i.e. it identifies more true Pareto optimal points faster (with smaller budget). Both BMA approaches’ performances are consistently in the range of the first best (F_2) single model’s performances. Complete results for all cases of N , swarm plots and coefficient plots for the multi-objective scenario may be found in the Supplementary figures.

V. DISCUSSION

A. Comparison of first-order and second-order BMA

From the results in the previous sections, we can see that for single-objective experiment design, the performance of the first-order BMA is slightly better than the second-order BMA. On the other hand, the model probabilities in the second-order BMA is more robust, and at any calculation number (sequential experiment iteration), the average posterior probability over all the initial data set instances of the best model in terms of experiment design performance is higher than the other models. The reason is that second-order Laplace approximation, unlike the first-order one, does not rely solely on the fitted values of the parameters of the GPR model to calculate the model probability. In fact, it approximates the model probability by integrating a local expansion of the marginal likelihood over a neighborhood of the fitted parameters values, which may dampen the fluctuations of the fitted values between different sequential experiment iterations. For the multi-objective case, the second-order BMA is slightly better than first-order BMA in terms of both experiment design performance and robustness of identifying the best model in terms of experiment design performance.

B. Remarks on feature sets

The feature sets in our analysis are chosen *a priori* based on domain knowledge. We do not claim that the considered feature sets are among the best possible feature sets for our experiment design problems. We are rather using these to showcase the applicability of the BOMU framework in real-world experiment design problems, where the best model or feature set is often not known, and only a set of possible models might exist based on domain knowledge. The power of BOMU is that it incorporates

the uncertainty over the possible model space, instead of relying on a single model that is selected based on limited initial available data. For instance, we compared experiment design results based on the subsets of F_2 with one feature removed from F_2 (by taking three features at a time): feature set F_{2a} : $[m, Z, I_{dist}]$, feature set F_{2b} : $[m, Z, e_a]$, feature set: F_{2c} : $[m, I_{dist}, e_a]$, and feature set F_{2d} : $[Z, I_{dist}, e_a]$.

Figs. 12a and 12b show the corresponding results for maximizing bulk modulus and minimizing shear modulus problems, respectively. From both figures, there are some subsets that can perform better in terms of average optimal objective values discovered over all instances of initial data sets for a fixed initial data set size. Another observation from Figs. 12a and 12b is that adding non-informative features to a model (feature set) can degrade the experiment design performance, as there are the single models based on some subsets of cardinality three derived from F_2 that can find the optimal compound in the MDS faster than the experiment design based on F_2 . One reason is that by adding non-informative features, more dimensions are introduced in the feature space while the information on these dimensions may be irrelevant to their outputs (it does not help better predict the outputs. This has more effect especially when using kernels with a single length-scale parameter, which is the most common practice in the materials literature. Further discussion is included in Sec. VIII

VI. CONCLUSIONS

The Bayesian optimization approach was successfully combined with Bayesian model averaging for autonomous and adaptive learning to design a Bayesian experiment design framework under model uncertainty (BOMU) for materials discovery in single- and multi-objective material property space using a test set of MAX phases. It was demonstrated that, while prior knowledge about the fundamental features linking the material to the desired material property is certainly essential to build the Materials Design Space (MDS), the BMA approach may be used to auto-select the *best* features/feature sets in the MDS, thereby eliminating the requirement of knowing the *best* feature set *a priori*. As evident from the extensive results included in the Supplementary figures, the BOMU framework is not significantly dependant on the size of the initial data, which enables its use in materials discovery problems where initial data is scant. At the very least, this framework provides a very efficient means of build-

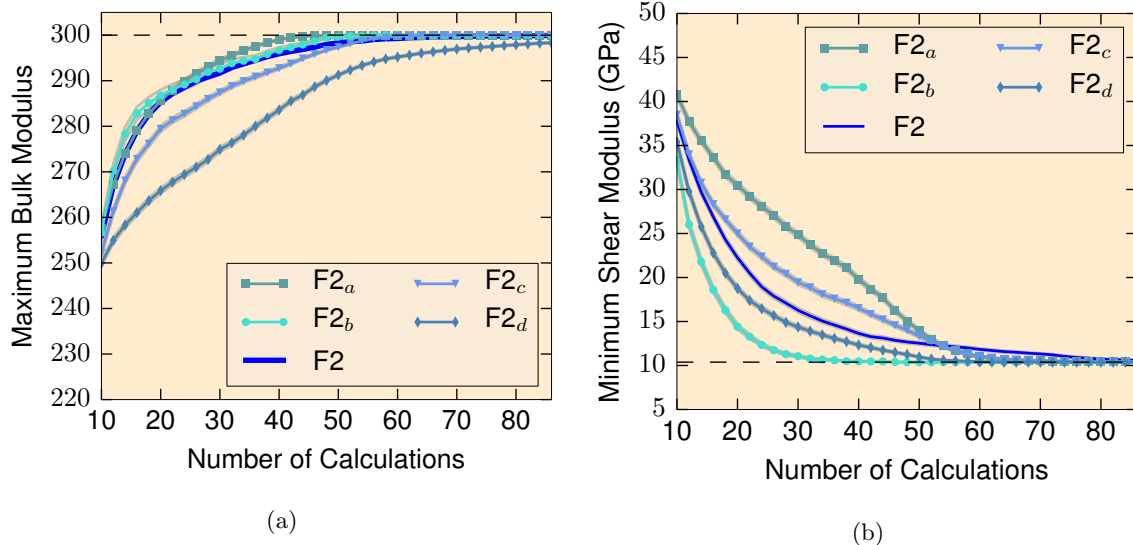


FIG. 12: Average maximum discovered a) bulk modulus and b) shear modulus for F_2 and lower-dimensional feature sets ($F_{2a}, F_{2b}, F_{2c}, F_{2d}$) derived from F_2

ing the initial data set as well, since it may be used to guide experiments or calculations by focusing on gathering data in those sections of the MDS which will result in the most efficient path to achieving the optimal material.

VII. ACKNOWLEDGMENTS

The authors acknowledge the support of NSF through the project *DMREF: Accelerating the Development of Phase-Transforming Heterogeneous Materials: Application to High Temperature Shape Memory Alloys*, NSF-CMMI-1534534. X.Q. acknowledges the support of NSF through the project *CAREER: Knowledge-driven Analytics, Model Uncertainty, and Experiment Design*, NSF-CCF-1553281. A.T. and R.A. also acknowledge support by the Air Force Office of Scientific Research under AFOSR-FA9550-78816-1-0180 (Program Manager: Dr. Ali Sayir).

A.T. and S.B. contributed equally to this work.

VIII. APPENDIX

The estimation of the (hyper) parameters, including the length-scale parameter, of the GPR model are found by maximizing the marginal likelihood of the data, i.e. ML-II estimation instead of the fully Bayesian treatment. Marginal likelihood might have multiple optima that correspond to different interpretations of the data. When GPR models are trained based on ML-II estimation, depending on the MDS and selected kernel functions, there is a possibility of overfitting the training data, especially when only a small number of measured data points are available (small-sample training data as initial data points). One thing to note is that experiment design based on GPR models that overfit the training data and assign very low correlation to nearby points in their prediction can yield very poor experiment design performance. One reason being that in this case measuring any point in the MDS will not give much information regarding other points of the MDS, because of the overfitting of the underlying learned surrogate GPR model. Since in our experiments the feature sets were chosen *a priori*, without any knowledge of their suitability for the underlying true model that generates data, in our implementation we have restricted the possible range for the length-scale parameter of the GPR kernel to prevent the models from overfitting the limited number of available data.

-
- [1] John P Holdren *et al.*, “Materials genome initiative for global competitiveness,” National Science and Technology Council OSTP. Washington, USA (2011).
- [2] National Research Council *et al.*, *Integrated computational materials engineering: a transformational discipline for improved competitiveness and national security* (National Academies Press, 2008).
- [3] Ankit Agrawal and Alok Choudhary, “Perspective: materials informatics and big data: realization of the fourth paradigm of science in materials science,” *APL Materials* **4**, 053208 (2016).
- [4] Surya R Kalidindi and Marc De Graef, “Materials data science: current status and future outlook,” *Annual Review of Materials Research* **45**, 171–193 (2015).
- [5] Radislav Potyrailo, Krishna Rajan, Klaus Stoewe, Ichiro Takeuchi, Bret Chisholm, and Hubert Lam, “Combinatorial and high-throughput screening of materials libraries: review of state of the art,” *ACS combinatorial science* **13**, 579–633 (2011).
- [6] Santosh K Suram, Joel A Haber, Jian Jin, and John M Gregoire, “Generating information-rich high-throughput experimental materials genomes using functional clustering via multitree genetic programming and information theory,” *ACS combinatorial science* **17**, 224–233 (2015).
- [7] Martin L Green, CL Choi, JR Hatrick-Simpers, AM Joshi, I Takeuchi, SC Barron, E Campo, T Chiang, S Empedocles, JM Gregoire, *et al.*, “Fulfilling the promise of the materials genome initiative with high-throughput experimental methodologies,” *Applied Physics Reviews* **4**, 011105 (2017).
- [8] Stefano Curtarolo, Gus LW Hart, Marco Buongiorno Nardelli, Natalio Mingo, Stefano Sanvito, and Ohad Levy, “The high-throughput highway to computational materials design,” *Nature materials* **12**, 191–201 (2013).
- [9] P Voorhees, G Spanos, *et al.*, *Modeling across scales: a roadmapping study for connecting materials models and simulations across length and time scales*, Tech. Rep. (Tech. rep., The Minerals, Metals & Materials Society (TMS), 2015).
- [10] Donald R Jones, Matthias Schonlau, and William J Welch, “Efficient global optimization of expensive black-box functions,” *Journal of Global optimization* **13**, 455–492 (1998).
- [11] Bobak Shahriari, Kevin Swersky, Ziyu Wang, Ryan P Adams, and Nando de Freitas, “Taking the human out of the loop: A review of bayesian optimization,” *Proceedings of the IEEE* **104**, 148–175 (2016).
- [12] Martin Pelikan, David E Goldberg, and Erick Cantú-Paz, “Boa: The bayesian optimization algorithm,” in *Proceedings of the 1st Annual Conference on Genetic and Evolutionary Computation-Volume 1* (Morgan Kaufmann Publishers Inc., 1999) pp. 525–532.
- [13] Koji Fujimura, Atsuto Seko, Yukinori Koyama, Akihide Kuwabara, Ippei Kishida, Kazuki Shitara, Craig AJ Fisher, Hiroki Moriwake, and Isao Tanaka, “Accelerated materials design of lithium superionic conductors based on first-principles calculations and machine learning algorithms,” *Advanced Energy Materials* **3**, 980–985 (2013).
- [14] Debasish Basak, Srimanta Pal, and Dipak Chandra Patranabis, “Support vector regression,” *Neural Information Processing-Letters and Reviews* **11**, 203–224 (2007).
- [15] Atsuto Seko, Tomoya Maekawa, Koji Tsuda, and Isao Tanaka, “Machine learning with systematic density-functional theory calculations: Application to melting temperatures of single- and binary-component solids,” *Physical Review B* **89**, 054303 (2014).
- [16] Carl Edward Rasmussen and Christopher KI Williams, *Gaussian processes for machine learning*, Vol. 1 (MIT press Cambridge, 2006).
- [17] Prasanna V Balachandran, Dezhen Xue, James Theiler, John Hogden, and Turab Lookman, “Adaptive strategies for materials design using uncertainties,” *Scientific reports* **6** (2016).
- [18] Michel W Barsoum, *MAX phases: properties of machinable ternary carbides and nitrides* (John Wiley & Sons, 2013).
- [19] Dezhen Xue, Prasanna V Balachandran, John Hogden, James Theiler, Deqing Xue, and Turab Lookman, “Accelerated search for materials with targeted properties by adaptive design,” *Nature communications* **7**, 11241 (2016).
- [20] Shenghong Ju, Takuma Shiga, Lei Feng, Zhufeng Hou, Koji Tsuda, and Junichiro Shiomi, “Designing nanostructures for phonon transport via bayesian optimization,” *Physical Review X* **7**, 021024 (2017).
- [21] Pavel Nikolaev, Daylond Hooper, Frederick Weber, Rahul Rao, Kevin Decker, Michael Krein, Jason Poleski, Rick Barto, and Benji Maruyama, “Autonomy in materials research: a case study in carbon nanotube growth,” *npj Computational Materials* **2**, 16031 (2016).
- [22] Turab Lookman, Prasanna V Balachandran, Dezhen Xue, John Hogden, and James Theiler, “Statistical inference and adaptive design for materials discovery,” *Current Opinion in Solid State and Materials Science* (2016).
- [23] Scott Broderick and Krishna Rajan, “Informatics derived materials databases for multifunctional properties,” *Science and technology of advanced materials* **16**, 013501 (2015).
- [24] M Botvinick, DGT Barrett, P Battaglia, N de Freitas, D Kumaran, JZ Leibo, T Lillicrap, J Modayil, S Mohamed, NC Rabinowitz, *et al.*, “Build-

- ing machines that learn and think for themselves: Commentary on lake et al., behavioral and brain sciences, 2017,” arXiv preprint arXiv:1711.08378 (2017).
- [25] Chao Sima and Edward R. Dougherty, “What should be expected from feature selection in small-sample settings,” *Bioinformatics* **22**, 2430 (2006).
- [26] Ulisses M Braga-Neto and Edward R Dougherty, “Is cross-validation valid for small-sample microarray classification?” *Bioinformatics* **20**, 374–380 (2004).
- [27] Jianping Hua, Waibhav D Tembe, and Edward R Dougherty, “Performance of feature-selection methods in the classification of high-dimension data,” *Pattern Recognition* **42**, 409–424 (2009).
- [28] David Madigan, Adrian E Raftery, C Volinsky, and J Hoeting, “Bayesian model averaging,” in *Proceedings of the AAAI Workshop on Integrating Multiple Learned Models, Portland, OR* (1996) pp. 77–83.
- [29] Jennifer A Hoeting, David Madigan, Adrian E Raftery, and Chris T Volinsky, “Bayesian model averaging: a tutorial,” *Statistical science* , 382–401 (1999).
- [30] Larry Wasserman, “Bayesian model selection and model averaging,” *Journal of mathematical psychology* **44**, 92–107 (2000).
- [31] Carl Edward Rasmussen and Christopher K. I. Williams, *Gaussian Processes for Machine Learning (Adaptive Computation and Machine Learning)* (The MIT Press, 2005).
- [32] Michael TM Emmerich, André H Deutz, and Jan Willem Klinkenberg, “Hypervolume-based expected improvement: Monotonicity properties and exact computation,” in *Evolutionary Computation (CEC), 2011 IEEE Congress on* (IEEE, 2011) pp. 2147–2154.
- [33] Miladin Radovic and Michel W Barsoum, “MAX phases: bridging the gap between metals and ceramics,” *American Ceramics Society Bulletin* **92**, 20–27 (2013).
- [34] Michel W Barsoum, “The $M_{N+1}AX_N$ phases: A new class of solids: Thermodynamically stable nanolaminates,” *Progress in Solid State Chemistry* **28**, 201–281 (2000).
- [35] M. W. Barsoum and M. Radovic, “Mechanical properties of the MAX phases,” in *Encyclopedia of Materials: Science and Technology*, edited by K. H. J. Buschow, R. Cahn, M. Flemings, B. Ilschner, E. Kramer, S. Mahajan, and P. Veyssiere (Elsevier, Amsterdam, 2004) pp. 1–16.
- [36] Michel W Barsoum and Miladin Radovic, “Elastic and mechanical properties of the MAX phases,” *Annual review of materials research* **41**, 195–227 (2011).
- [37] ZM Sun, “Progress in research and development on MAX phases: A family of layered ternary compounds,” *International Materials Reviews* **56**, 143–166 (2011).
- [38] MW Barsoum, “The MAX Phases and Their Properties in Ceramics Science and Technology,” (2010).
- [39] R Arróyave, A Talapatra, T Duong, W Son, H Gao, and M Radovic, “Does aluminum play well with others? intrinsic al-a alloying behavior in 211/312 MAX phases,” *Materials Research Letters* , 1–9 (2016).
- [40] Anjana Talapatra, T Duong, W Son, H Gao, M Radovic, and R Arróyave, “High-throughput combinatorial study of the effect of m site alloying on the solid solution behavior of M_2AlC MAX phases,” *Physical Review B* **94**, 104106 (2016).
- [41] Sitaram Aryal, Ridwan Sakidja, Michel W Barsoum, and Wai-Yim Ching, “A genomic approach to the stability, elastic, and electronic properties of the MAX phases,” *Physica Status Solidi (B)* **251**, 1480–1497 (2014).
- [42] Fabian Pedregosa, Gaël Varoquaux, Alexandre Gramfort, Vincent Michel, Bertrand Thirion, Olivier Grisel, Mathieu Blondel, Peter Prettenhofer, Ron Weiss, Vincent Dubourg, *et al.*, “Scikit-learn: Machine learning in python,” *Journal of machine learning research* **12**, 2825–2830 (2011).
- [43] Y Makino and S Miyake, “Estimation of bulk moduli of compounds by empirical relations between bulk modulus and interatomic distance,” *Journal of alloys and compounds* **313**, 235–241 (2000).
- [44] J Karthikeyan, Vijay Kumar, and P Murugan, “The role of valence electron concentration in tuning the structure, stability, and electronic properties of mo_6s_9-x i x nanowires,” *The Journal of Physical Chemistry C* **119**, 13979–13985 (2015).
- [45] Sheng Guo, Chun Ng, Jian Lu, and C. T. Liu, “Effect of valence electron concentration on stability of fcc or bcc phase in high entropy alloys,” *Journal of Applied Physics* **109**, 103505 (2011).
- [46] U Mizutani and H Sato, “Determination of electrons per atom ratio for transition metal compounds studied by flapw-fourier calculations,” *Philosophical Magazine* **96**, 3075–3096 (2016).
- [47] Sander Pronk and Daan Frenkel, “Large difference in the elastic properties of fcc and hcp hard-sphere crystals,” *Physical review letters* **90**, 255501 (2003).
- [48] Desmond Tromans, “Elastic anisotropy of hcp metal crystals and polycrystals,” *Int. J. Res. Rev. Appl. Sci* **6**, 462–483 (2011).
- [49] David R Lide *et al.*, “Crc handbook of chemistry and physics,” 12J204 (1998).
- [50] Kirthevasan Kandasamy, Jeff Schneider, and Barnabás Póczos, “High dimensional bayesian optimisation and bandits via additive models,” in *International Conference on Machine Learning* (2015) pp. 295–304.
- [51] László Györfi, Michael Kohler, Adam Krzyzak, and Harro Walk, *A distribution-free theory of nonparametric regression* (Springer Science & Business Media, 2006).
- [52] Adam D Bull, “Convergence rates of efficient global optimization algorithms,” *Journal of Machine Learning Research* **12**, 2879–2904 (2011).

- [53] Ziyu Wang, Frank Hutter, Masrour Zoghi, David Matheson, and Nando de Feitas, “Bayesian optimization in a billion dimensions via random embeddings,” *Journal of Artificial Intelligence Research* **55**, 361–387 (2016).
- [54] K Pearson, “Notes on regression and inheritance in the case of two parents proceedings of the royal society of london, 58, 240-242,” (1895).
- [55] Walter Kohn and Lu Jeu Sham, “Self-consistent equations including exchange and correlation effects,” *Physical review* **140**, A1133 (1965).
- [56] Georg Kresse and Jürgen Furthmüller, “Efficient iterative schemes for ab initio total-energy calculations using a plane-wave basis set,” *Physical Review B* **54**, 11169 (1996).
- [57] Georg Kresse and Jürgen Furthmüller, “Efficiency of ab-initio total energy calculations for metals and semiconductors using a plane-wave basis set,” *Computational Materials Science* **6**, 15–50 (1996).
- [58] John P Perdew and Yue Wang, “Accurate and simple analytic representation of the electron-gas correlation energy,” *Physical Review B* **45**, 13244 (1992).
- [59] John P Perdew, Kieron Burke, and Matthias Ernzerhof, “Generalized gradient approximation made simple,” *Physical Review Letters* **77**, 3865 (1996).
- [60] John P. Perdew, Kieron Burke, and Matthias Ernzerhof, “Generalized gradient approximation made simple,” *Physical Review Letters* **78**, 1396–1396 (1997).
- [61] Hendrik J Monkhorst and James D Pack, “Special points for brillouin-zone integrations,” *Physical Review B* **13**, 5188 (1976).
- [62] MPAT Methfessel and AT Paxton, “High-precision sampling for brillouin-zone integration in metals,” *Physical Review B* **40**, 3616 (1989).
- [63] Peter E Blöchl, Ove Jepsen, and Ole Krogh Andersen, “Improved tetrahedron method for brillouin-zone integrations,” *Physical Review B* **49**, 16223 (1994).
- [64] Yvon Le Page and Paul Saxe, “Symmetry-general least-squares extraction of elastic data for strained materials from ab initio calculations of stress,” *Physical Review B* **65**, 104104 (2002).
- [65] Navdeep Singh, Anjana Talapatra, Anchalee Junkaew, Thien Duong, Sean Gibbons, Shengyen Li, Hassan Thawabi, Emmi Olivos, and Raymundo Arróyave, “Effect of ternary additions to structural properties of niti alloys,” *Computational Materials Science* **112**, 347–355 (2016).
- [66] Thien Duong, Sean Gibbons, Rajeev Kinra, and Raymundo Arrayave, “Ab-initio approach to the electronic, structural, elastic, and finite-temperature thermodynamic properties of ti2ax (a=al or ga and x=c or n),” *Journal of Applied Physics* **110**, 093504 (2011).
- [67] Richard Hill, “The elastic behaviour of a crystalline aggregate,” *Proceedings of the Physical Society. Section A* **65**, 349 (1952).
- [68] P. Sirisalee, M.F. Ashby, G.T. Parks, and P.J. Clarkson, “Multi-criteria material selection in engineering design,” *Advanced Engineering Materials* **6**, 84–92 (2004).